Appl. Phys. B 80, 377–387 (2005)
DOI: 10.1007/s00340-004-1720-2

Applied Physics B
Lasers and Optics

D.N. KOZLOV

Simultaneous characterization of flow velocity and temperature fields in a gas jet by use of electrostrictive laser-induced gratings

A.M. Prokhorov General Physics Institute, Russian Academy of Sciences,
38 Vavilov str., 119991 Moscow, Russia

Received: 21 July 2004/Revised version: 19 November 2004
Published online: 21 December 2004 •

ABSTRACT Time-resolved light diffraction of cw read-out laser radiation by electrostrictive laser-induced gratings (LIGs) is demonstrated to be applicable, under a special experimental arrangement, for non-intrusive, local, and remote simultaneous measurements of velocity and temperature in gas flows. The experimental set-up and the model developed for adequate description of the experimental results are described. The method for treating the data and estimating the experimental parameters is reported.

The demonstrative, proof-of-principle experiments were performed under stationary flow conditions in plane submerged heated air jet in atmosphere at ambient pressure and temperature. Phase-sensitive detection of the diffracted light was accomplished by superimposing two signal beams, whose frequencies were Doppler-shifted by the movement of the grating together with the flow. Flow velocities in the range 10–160 m/s and temperatures between ambient and 600 K were measured, and profiles of the corresponding values along and across the jet were demonstrated to be obtainable. In addition to velocity and temperature values, characteristic longitudinal and transversal spatial distributions of such a parameter as a LIG signal decay time were obtained. These data may provide information on the turbulent movement inside the flow and on the jet structure.

PACS 42.62.-b; 47.62.+q; 43.58.+z

1 Introduction

During recent years a significant amount of studies appeared, devoted to demonstration and assessment of possibilities to employ diffraction by laser-induced gratings (LIGs) [1–9] and related phenomena of four-photon light–matter interaction, like degenerate four-wave mixing (DFWM) [10] and coherent anti-Stokes Raman scattering (CARS) [11–14], for measurements of flow velocities and temperature in gases. The interest to these investigations is due to the fact that these methods allow to accomplish local velocimetry and thermometry simultaneously and non-intrusively, without seeding the gas with scattering particles, as it is usually done in the traditional methods of laser Doppler anemometry (LDA) [15, 16]. Moreover, simultaneous measurements in a single laser shot provide possibilities to investigate velocity–temperature correlations in turbulent flows that are of importance for numerical modeling of the relevant processes.

Laser-induced gratings are spatial modulations of the complex refractive index of a medium produced by the field of the interference pattern, which is formed by two equally polarized pump laser beams [17]. The gratings can be efficiently read out using Bragg diffraction of radiation from another laser. In the studies employing LIGs, the investigations of both spectrum of the diffracted radiation [1] and temporal evolution of its power, with homodyne [2, 5, 6] or heterodyne [3, 4, 7–9] detection of the optical signal and subsequent time-domain [2–7] or frequency-domain [7–9] data analysis, were being accomplished.

In our first experiments using the laser-induced gratings technique for flow diagnostics [3], the possibility of applying electrostrictive LIGs [18] for simultaneous velocity and temperature measurements was demonstrated in the laboratory for plane jets of air blown out of the slot nozzle into atmosphere at ambient temperature and pressure. The advantage of electrostrictive LIGs is that they can be non-resonantly excited in various test gases by any pulsed laser. In [3] LIGs were "instantaneously" generated partly inside and partly outside the jet and read out using a cw probe beam. Time-domain analysis of the diffracted light power temporal evolution was employed to determine the flow velocity and temperature. The values were measured near the exit of the nozzle as a function of the averaged exit velocity. The LIG signals were recorded using a version of a heterodyne signal detection scheme, where the beam diffracted outside the flow was providing in fact a reference beam. The disadvantage of this experimental arrangement was its low spatial resolution defined by the large length of the probe volume.

Further experiments were aimed at the development and assessment of the approaches that allow one to employ LIGs with the effective length smaller than the width of the flow and thus to enhance the spatial resolution of the technique in application to our purposes. First, two counter-propagating read-out beams were arranged to generate two diffracted light waves with the opposite sign of the Doppler frequency shift resulting from the movement of a LIG with the flow [5]. The diffracted beams were made to spatially overlap, enabling

✉ Fax: +7-095-135-02-97, E-mail: dnk@kapella.gpi.ru

their interference. The flow velocity was determined from the beat frequency in a LIG signal temporal evolution. The period of the higher-frequency signal oscillation was simultaneously employed for temperature measurements. Second, another modification of the experimental scheme, employing a frequency-shifted reference laser beam and based on heterodyne-detection of the signal, has been developed and later on tested in a large-scale supersonic experimental facility [8]. In more details this approach is described in a recent paper [19].

The proof-of-principle simultaneous flow velocity and temperature measurements (both single-shot and temporally averaged) using the counter-propagating read-out beams [5] have been initially performed at the axis of the jet near the orifice of the laboratory slot nozzle, that was producing the flow under investigation. In the subsequent work the experiments aimed to demonstrate possibilities of point-to-point measurements across and along the heated jets have been conducted. Mainly temporally-averaged measurements have been performed. The present paper describes in detail the experimental results obtained and the theoretical model developed for data evaluation. It shows the possibilities and limitations of the LIG technique to provide information on spatial distributions of temperature and velocity inside the flow. The data on the spatial and temperature-dependent variations of the LIG signal decay time inside the flow are also presented, giving a promise to employ the technique for characterization of flow turbulence. This possibility might be of interest for verification of turbulent flow models.

2 Experimental

In a LIG experiment electrostrictive gratings are produced by two equally polarized pulsed pump laser beams with an arbitrary wavelength λ_P and the wave vectors $\boldsymbol{k_1}$ and $\boldsymbol{k_2}$, that intersect at a small angle θ_P and interfere. The fringe spacing of the interference pattern is $\Lambda = \lambda_P/2\sin(\theta_P/2) = 2\pi/|\boldsymbol{q}|, \boldsymbol{q} = \boldsymbol{k_1} - \boldsymbol{k_2}$. The effective length of the volume excited by the pump beams, d (the length of the grating), can be estimated as $d \cong \sqrt{2}\Lambda(2w_0/\lambda_P)$, where $2w_0$ is the $1/e^2$-level diameter of the Gaussian intensity profile of the pump beams in the crossing area. For efficient Bragg diffraction, the laser radiation reading out a LIG, with a wavelength λ_R, should be directed to the planes of the fringes at the angle θ_R defined by the relation:

$$\sin\theta_R = (\lambda_R/\lambda_P)\sin(\theta_P/2)\,.$$

The known requirement for Bragg diffraction $\lambda_R d/\Lambda^2 > 1$, expressed in our case as $\sqrt{2}(\lambda_R/\lambda_P)(2w_0/\Lambda) > 1$, can be easily satisfied by the appropriate choice of λ_P, λ_R, $2w_0$ and the geometry of the experiment.

To conduct the electrostrictive LIG experiments with the oppositely directed read-out beams the standard LIG set-up used previously [3, 18] had been modified as shown in Fig. 1. The pump radiation at $\lambda_P = 1064$ nm provided by a pulsed Nd:YAG laser (Continuum, NY81-20, output energy ≈ 80 mJ/pulse, repetition rate 20 Hz, $\Delta\nu \approx 1.1$ cm^{-1}, pulse length $\tau_P \approx 8$ ns), with the beam diameter of about 8 mm, was focused using a lens L_1 ($f = 1000$ mm). A beam splitter BS placed just behind the lens produced two pairs of

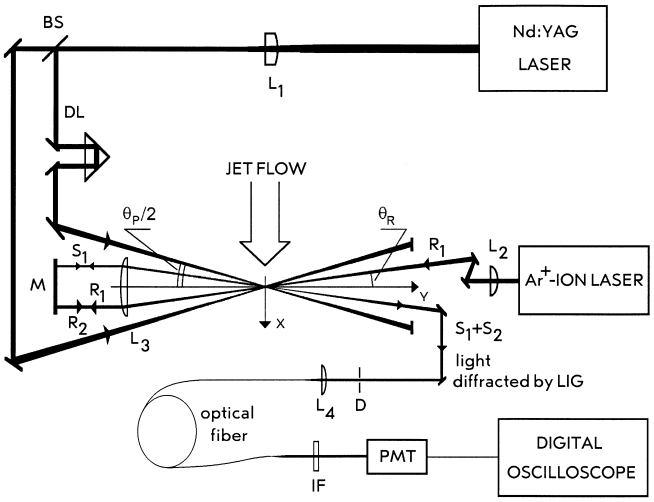

FIGURE 1 The scheme of the experimental set-up: BS - beam splitter; L_1–L_4 - lenses; DL - delay line; M - retro-reflecting mirror; PMT - photomultiplier tube; D - diaphragm; IF - interference filter; R_1, R_2 - read-out beams; S_1, S_2 - signal beams

roughly equally intense excitation beams of parallel polarizations. The adjustable delay line DL ensured the appropriate temporal overlap of the pump laser pulses (i.e., corresponding to their coherence length) in the beams crossing point. To decrease the length of LIGs, the beams were aligned to cross each other at a larger than in [3] angle $\theta_P \approx 2.63°$ resulting in a fringe spacing $\Lambda \approx 23.2$ μm. In the focal region the $1/e^2$-level diameters of the Gaussian pump beams were measured to be $2w_0 \approx 300$ μm, that provided the effective length of the grating of about 10 mm.

The cw radiation of an Ar^+-ion laser at $\lambda_R = 514.5$ nm (Spectra-Physics, BeamLok M2060-5S, power ≈ 0.9 W), used to read-out laser-induced gratings, was focused into the centre of the crossing region of the pump beams by a lens L_2 ($f = 1000$ mm), with the focal spot diameter, $2w_R$, slightly smaller than that of the pump beam. This radiation was directed at $\theta_R \approx 0.64°$ to the planes of the interference fringes, satisfying the Bragg condition in a 3-D backward phase-matching geometry, and produced the forward-diffracted signal beam (beams R_1 and S_1, respectively, in Fig. 1). In this case, the probe volume had a quasi-cylindrical shape defined by the overlap region of the two pump and read-out laser beams, with a longitudinal dimension expected to be slightly smaller than the grating length $d \approx 10$ mm. After passing through the flow, the read-out radiation was recollimated by a lens L_3 ($f = 1000$ mm) and was reflected back to the probe volume by a flat mirror M at the same Bragg angle to the optical axis. In this way the retro-reflected beam (R_2) was employed as an oppositely directed read-out beam producing the backward-diffracted signal beam S_2. The same lens L_3 and mirror M were used to recollimate and retro-reflect, respectively, the beam S_1 in such a way that it appeared to be spatially overlapped with the beam S_2.

The pulses of coherent light of the overlapped signal beams, diffracted by LIGs, were directed to the iris diaphragm D and then focused into a multimode optical fiber with 120 μm of core diameter. The fiber was used as a spatial filter reducing background scattered light of the read-out radiation.

The signal radiation was passing through an interference filter IF and was detected by a photomultiplier PMT (Philips, XP2020). The temporally resolved signals were recorded using a digital oscilloscope (Tektronix, TDS 744A) with a full bandwidth of 500 MHz and a sampling rate up to 2 GHz.

Since the signal beams S_1 and S_2 were diffracted from the same read-out beam within its coherence length, being spatially overlapped they interfere at the photodetector. In this case, the diffracted light of the beam S_1 was found to be delayed, as related to that of the beam S_2, by about 8 ns needed for the beam S_1 to travel forth and back until it became overlapped with the beam S_2. Note, that the frequencies of light diffracted into the beams S_1 and S_2 by the LIG generated in a flow should have the opposite sign of the Doppler shift originating from the movement of the medium along the direction of the grating vector $\boldsymbol{q}$, since the wave vectors of the beams R_1 and R_2 had opposite projections on $\boldsymbol{q}$. As a result, the corresponding beat frequency in the temporal evolution of a LIG signal could be observed and employed to deduce the flow velocity component parallel to $\boldsymbol{q}$.

To obtain, for preliminary investigations, plane jets with variable, but definite velocity and temperature fields under stationary flow conditions, a dry air supply system available in the laboratory and a simple heatable slot nozzle were employed. The nozzle was produced by flattening an end of a copper tube 200 mm in length and 15 mm in inner diameter. Thus, the tube ended in a plane nozzle about 20 mm in length, with the orifice height $h = 1.5$ mm and width $l = 22$ mm. The nozzle cross section at the exit was equal to $S_N \approx 32.5\,\text{mm}^2$. The jets were submerged in atmosphere at ambient pressure and temperature. The volume rates of air flow were measured at ambient temperature using a flow-meter in a gas supply before the entrance to the nozzle and were varied over a range of 20–200 l/min. The corresponding averaged flow velocities at the exit of the nozzle, v_Q, calculated as $v_Q = Q/S_N$ from the measured flow rates and the nozzle cross-section, were changing from 10 to 100 m/s (at ambient temperature). The resistance heater had been placed around the walls of the copper tube providing variable heating up to 1100 K. The wall temperature was controlled with a thermocouple. Different gas temperatures $T_{ex} = 295$–600 K at the jet axis near the nozzle orifice, as measured by the thermocouple inserted into the flow, were employed. In the axial plane of the jet gas temperatures at the nozzle exit were checked to be constant within 1% at the length of about 20 mm along the orifice.

Reynolds number inside the channel of the slot nozzle near its exit can be calculated as $Re = \varrho v_Q h/\mu$ [20], where ϱ is the equilibrium (i.e., spatially homogeneous) gas density and μ is the dynamic gas viscosity. This relation reduces to $Re \cong v_Q[\text{m/s}] \times 10^2$ for air at ambient temperature and pressure. Thus, the estimates of Reynolds numbers at the nozzle exit give the values $Re \approx 10^3 - 10^4$ for the flows employed at $T_{ex} = 295$ K. Assuming that a flow in the channel of the nozzle is similar to a fully developed pipe flow, the critical Reynolds number should be about $Re \approx 2 \times 10^3$ [20, 21]. Hence, one can expect that the investigated range of flow rates corresponds to transition from quasi-laminar (at about $Q = 20$ l/min) to turbulent free jets (at $Q \geq 40$ l/min). Considering that the characteristic integral turbulent length scale equals to h, the Kolmogorov length of the low-scale turbulence can be estimated as $\lambda_0 \approx h\,Re_t^{-3/4}$ [20, 21]. Here the turbulent Reynolds number, Re_t, is defined by the turbulent kinetic energy rather than mean velocity. Since typically $Re_t \sim 10^{-2}$–$10^{-1}\,Re$ in a pipe flow [21], in our case $\lambda_0 \ll 270\,\mu$m. Hence, turbulent pulsations are averaged over the probe volume.

The axes of the laboratory-fixed coordinate system were defined as follows (see Fig. 1): the x-axis was coincident with the symmetry axis of the nozzle and was pointing in the main flow direction, and the y- and z-axes were lying in the plane of the nozzle orifice, the y-axis being parallel to its wide side. Hence, the origin of the coordinate system was located at the centre of the orifice. The pump and read-out beams were adjusted to lie parallel to the x–y-plane. Their crossing point (centre of the probe volume) was located in the x–z plane in such a way that the optical axis was parallel to the y-axis and the grating vector $\boldsymbol{q}$ was parallel to the x-axis.

The alignment of the crossing of the pump and read-out beams and of the detection system was carried out using diaphragms and a pin-hole located at the position of the beam waists. The set-up adjustment, optimization and test of operation was performed during measurements with LIGs in room air by detection of one of the signal beams (S_1 or S_2) or two beams together. The measurements in the flow were performed with the probe volume centred in the x–z plane at various positions across the jet (along the z-axis) and at various distances from the plane of the nozzle orifice, the closest distance being equal to about 0.9 mm ($x/h = 0.6$). The lengths of the excitation and the probe volumes ($d \approx 10$ mm) were smaller than the width of the slot ($l = 22$ mm), and hence the fringes of LIGs were located completely inside the jet flow.

3 LIG signal temporal profile: data analysis approach

Electrostrictive laser-induced gratings are generated when the electric field of the interference pattern of two short-pulse pump laser beams polarizes the medium, and the spatially periodic inhomogeneity of the field exerts a force resulting in the corresponding variations of density [18, 22, 23]. The efficiency η of Bragg diffraction by a LIG in the absence of absorption of the read-out beam at the wavelength λ_R is expressed in a gas as [17]:

$$\eta = \frac{P_S}{P_R} = \left[\frac{\pi d}{\lambda_R}\delta n\right]^2 \approx \left[\frac{\pi d}{\lambda_R}\left(\frac{\partial n}{\partial \varrho}\right)_T \delta\varrho\right]^2 . \qquad (1)$$

Here, P_S and P_R are the powers of the diffracted and read-out laser beams, while n and ϱ, δn and $\delta\varrho$ are the equilibrium refractive index and gas density and their variations across a fringe of the grating, respectively, and d, as above, is a length of the grating. Equation (1) takes into account that in a gas the weak dependence of the refractive index on temperature can be neglected as compared to the change of n due to variation of gas density.

The density variations affected by electrostriction can be quantitatively described using the linearized hydrodynamic equations [18, 22, 23]. The solution of these equations, that is obtained under the conditions of weak acoustic damping,

is a superposition of acoustic waves, created by electrostrictive adiabatic compression of the medium, and acoustic and stationary density modulations, due to the local temperature variation resulting from the adiabatic compression. The wavelength of the acoustic waves is defined by the fringe spacing of the interference pattern, Λ. The acoustic waves propagate in opposite directions with the wave vectors $\boldsymbol{q}$ and $-\boldsymbol{q}$, normal to the planes of the fringes, have equal amplitudes, and spatially overlap. Hence, a standing acoustic wave, i.e., a spatially periodic density modulation oscillating in time, appears. This is accompanied, in accordance with (1), by the respective oscillation of the diffraction efficiency η, if the LIG is read out.

Under the conditions of weak damping, the density modulations due to temperature variations are small compared to those caused by the adiabatic compression directly [23], and hence can be neglected. As a result, in case of the "instantaneous" excitation by an infinitely short laser pulse at the initial moment $t = 0$ the approximate expression for the spatial and temporal variation $\Delta\varrho$ of the equilibrium gas density can be written at $t > 0$ as

$$\Delta\varrho \cong A\left[\sin \Omega t \exp(-t/\tau_\mathrm{a})\right] \Theta(t) \cos(\boldsymbol{qr}) \,, \tag{2}$$

where the frequency of the acoustic wave $\Omega = 2\pi v_\mathrm{s}/\Lambda \equiv 2\pi/T_\mathrm{a}$ is defined by the adiabatic sound velocity v_s, and T_a is the acoustic wave period, τ_a is the damping constant of the acoustic wave, $\Theta(t)$ is the Heaviside step function. The scale factor A in (2) is defined as (see [18]):

$$A = \gamma_\mathrm{e} \frac{2\pi}{\Lambda v_\mathrm{s} c} \left[(W_1 W_2)^{1/2}/S\right] \,. \tag{3}$$

Here, $\gamma_\mathrm{e} = \varrho\,(\partial\varepsilon/\partial\varrho)$ denotes the electrostrictive constant, with ε being the equilibrium dielectric constant, c is the speed of light, $W_{1,2}$ are the pump pulse energies, and S is the cross section of the pump beams. Note that finite (focused) pump beams create a pair of spatially limited acoustic wave packets, that overlap in space and form a purely standing wave only at the initial moment and diverge later on.

The amplitude of an acoustic wave in a gas is damped due to viscosity and heat conduction. The time constant τ_a scales as Λ^2 and is proportional to the gas density ϱ [18, 23], so that the conditions of weak acoustic damping, expressed as $T_\mathrm{a}/2\pi \ll \tau_\mathrm{a}$, are fulfilled the better the higher is the density. However, in the experiments with the focused beams the oscillation of η usually decays faster, than is expected from the estimate of τ_a value. In this case the decay time constant is primarily determined by the rate of the relative displacement of the two counter-propagating and initially overlapped acoustic wave packets. For beams with a Gaussian profile of the transversal intensity distribution and similar beam diameters $2w_\mathrm{R} \leq 2w_0$ the decay of the oscillation of the LIG diffraction efficiency due to this displacement can be characterized by the parameter $\tau_\mathrm{tr} = w_0/\sqrt{2}v_\mathrm{s}$ (acoustic transit time). The effect can be quantitatively described with reasonable accuracy by introducing the damping factor $\exp\left(-t/\tau_\mathrm{a} - t^2/\tau_\mathrm{tr}^2\right)$, instead of $\exp(-t/\tau_\mathrm{a})$, in (2). If $\tau_\mathrm{tr} \ll \tau_\mathrm{a}$, the influence of τ_a obviously becomes negligible.

The more strict and physically successive analysis of the LIG signal temporal evolution, that takes into account finite transversal dimensions and probably slight misalignment of the beams, should follow the elaborate approach presented in [2]. However, in a simplified way the temporal evolution of a signal from the moving medium, obtained in the experiment with two oppositely directed read-out beams, can be reasonably described in the plane-wave approximation assuming the infinite beams, as follows. The fields E_{R_1} of the forward-directed and E_{R_2} of the back-reflected read-out beams R_1 and R_2 (see Fig. 1), with a wavelength λ_R, and the fields E_{S_1} and E_{S_2} of light Bragg-diffracted in forward (beam S_1) and backward (beam S_2) directions, respectively, can be expressed as

$$\begin{aligned} E_{R_{1,2}}(\boldsymbol{r}, t) &= E_{R_{1,2}}(t) \exp(-\mathrm{i}\omega_\mathrm{R} t \pm \mathrm{i}\boldsymbol{k}_\mathrm{R}\boldsymbol{r}) + c.c.\,, \\ E_{S_{1,2}}(\boldsymbol{r}, t) &= E_{S_{1,2}}(t) \exp\left(-\mathrm{i}\omega_\mathrm{R} t \pm \mathrm{i}\boldsymbol{k}_{S_1}\boldsymbol{r}\right) + c.c\,. \end{aligned} \tag{4}$$

Here $E_{R_{1,2}}(t)$ and $E_{S_{1,2}}(t)$ are the complex amplitudes, $\boldsymbol{k}_\mathrm{R}$ and $\boldsymbol{k}_{S_1} = \boldsymbol{k}_\mathrm{R} - \boldsymbol{q}$ are the wave vectors of the forward-directed read-out and diffracted beams, respectively, with $\boldsymbol{k}_{S_2} = -\boldsymbol{k}_{S_1}$, and ω_R is the angular frequency of the read-out radiation.

The density modulation, "instantaneously" generated by the pump beams at $t = 0$ through electrostriction and described by (2), under assumption that equilibrium temperature and density are constant along the y-axis at the length of the grating d, defines the complex amplitudes $E_{S_{1,2}}(t)$ of the diffracted light, in accordance with [24], as

$$E_{S_{1,2}}(t) \propto E_{R_{1,2}}(t) d\Delta\varrho \propto E_{R_{1,2}}(t) \sin \Omega t \exp(-t/\tau_\mathrm{a})\Theta(t) \,. \tag{5}$$

Respectively, in the medium that moves with the velocity $\boldsymbol{v}$, the complex amplitudes $E_{S_{1,2}}(t)$ of the diffracted light waves can be expressed as

$$E_{S_{1,2}}(t) \propto E_{R_{1,2}}(t) \exp(\pm\mathrm{i}\boldsymbol{qv}t) \sin \Omega t \exp(-t/\tau_\mathrm{a})\Theta(t) \,. \tag{5'}$$

Combining with (4), one can see that the frequency of light diffracted from inside the flow experiences Doppler shifts $\pm\boldsymbol{qv}$ from the frequency ω_R of the read-out beam, and these shifts are proportional to the component of the flow velocity, v_q, along $\boldsymbol{q}$ (the x-axis): $\boldsymbol{qv} = (2\pi/\Lambda)\, v_q = \left(v_q/v_{\mathrm{s}0}\right) \Omega_0$. Here, index 0 refers to the medium at ambient (calibration) temperature and pressure, where the sound velocity $v_{\mathrm{s}0}$ is also supposed to be known. Inside the flow the sound velocity v_s, and hence the frequency Ω of the acoustic wave, is determined by the local gas parameters.

After the back reflection of the beam R_1 by the mirror M and spatial overlapping of the two diffracted coherent beams, at $t > t_1$, where t_1 is the time needed for the beam R_1 to travel forth from the probe volume to the retro-reflecting mirror M and back, the total diffracted radiation field appears to be a sum of the two contributions. The complex amplitude of this field is $E_\mathrm{S}(t) = E_{S_1}(t - t_1)\exp(\mathrm{i}\varphi) + E_{S_2}(t)$, where φ is an arbitrary phase shift between the interfering waves. The temporal evolution of the total diffracted power P_s (or the photodetector signal) is obtained by integrating the diffracted light intensity, proportional to $E_S E_S{}^*$, over the cross section

of the diffracted beam:

$$\begin{aligned} P_S(t) &\propto \int (E_S E_S^*)\,\mathrm{d}S = A\sin^2\Omega(t-t_1)\exp(-2(t-t_1)/\tau_a) \\ &+ B\sin^2\Omega t\exp(-2t/\tau_a) + 2C\cos(2(v_q/v_{s0})\Omega_0 t+\psi) \\ &\times \sin\Omega(t-t_1)\sin\Omega t\exp(-(t-t_1)/\tau_a - t/\tau_a) \\ &= A\left[\sin^2\Omega(t-t_1)\exp(-2(t-t_1)/\tau_a) + K\sin^2\Omega t\right. \\ &\times \exp(-2t/\tau_a) + 2K_i\cos(\Omega_m t+\psi)\sin\Omega(t-t_1) \\ &\left.\times \sin\Omega t\exp(-(t-t_1)/\tau_a - t/\tau_a)\right], \end{aligned} \tag{6}$$

where the coefficients A, B and C, proportional to d^2, are determined by the pump beams pulse energies, power of the read-out beams R_1 and R_2 and properties of the medium, $K=(B/A)$, $K_i=C/A$ and ψ is an arbitrary phase shift. Thus, a high-frequency (2Ω) oscillation in the temporal profile of a LIG signal is amplitude-modulated, due to the Doppler effect, with the low frequency $\Omega_m = 2(v_q/v_{s0})\Omega_0$, proportional to the x-component of the flow velocity. If $t_1 \ll T_a$, τ_a, (6) reduces to

$$\begin{aligned} P_S(t) &\propto \\ &A\,(1+K)\,[1+m\cos(\Omega_m t+\psi)]\sin^2\Omega t\exp(-2t/\tau_a)\,, \end{aligned} \tag{7}$$

where the modulation coefficient m is defined as $2K_i/(1+K)$.

The transit times for the two counter-propagating acoustic wave packets leaving the probe volume become different: $\tau_{tr1} = w_0/\sqrt{2}(v_s - v_q)$, $\tau_{tr2} = w_0/\sqrt{2}(v_s + v_q)$. Under the assumptions that flow velocities are not high, i.e., $v_q \ll v_s$, so that the dependence of τ_{tr} on v_q can be neglected, and that the read-out beam diameter w_R is smaller than w_0, to describe the effect of this divergence quantitatively one can, as before, to replace the damping factor $\exp(-t/\tau_a)$ in (5)–(7) by $\exp(-t/\tau_a - t^2/\tau_{tr}^2)$.

In accordance with (6),(7), the temporal evolution of the power of the beam, diffracted by the standing acoustic wave, shows a regular high-frequency oscillation with a period $\pi/\Omega = T_a/2$. By deriving the acoustic wave period T_a from a LIG signal and assuming that the fringe spacing Λ remains constant with pressure and temperature one can determine the adiabatic sound velocity $v_s = \Lambda/T_a$. In an ideal gas v_s is independent on pressure and is given by the known relation

$$v_s = \sqrt{\gamma\frac{R}{M}T}\,, \tag{8}$$

where T denotes the temperature, $\gamma = c_P/c_V$ is the ratio of the specific heat at constant pressure and volume, M is the molar mass, and R is the universal gas constant. Thus, if the gas composition is known, and the dependence of γ on temperature is weak, with (8) one can calculate temperature. At a given gas composition relative temperature measurements, that refer to the value Ω_0 defined at known calibration temperature, can be performed as well. Note, that in a real gas there is a weak dependence of v_s on pressure.

Therefore, simultaneous measurements of flow velocity and temperature using electrostrictive LIGs excited inside the flow can be realized in the presented experimental arrangement. They can be accomplished by deriving the values $\Omega_m = 2(v_q/v_{s0})\Omega_0$ and $\Omega \cong \Omega_0\sqrt{T/T_0}$ from the same single-shot or temporally-averaged signal as a result of fitting its temporal evolution using (6) or (7), where the appropriate temperature dependence of τ_a and τ_{tr} is introduced, and employing the known values of v_{s0} and Ω_0.

The spatial resolution of the LIGs technique along the y-axis (the bisectrix of angle θ_P) is determined by the effective length of the probe volume, which in our case of $\theta_R < \theta_P/2$ and $w_R \le w_0$ practically equals to the length of the grating d. Since $d \sim \Lambda w_0$, the spatial resolution can be improved, if required (i.e., d can be decreased), at the expense of a reduction of Λ, by enhancement of the intersection angle θ_P, and/or a reduction of w_0, by tighter focusing of the pump beams. Employing (1)–(3), it can be easily shown that for the diffraction efficiency of an electrostrictive LIG the relation $\eta \sim (d\delta\varrho)^2 \sim w_0^{-2}$ is valid, if $w_R \approx w_0$ holds. Thus, with the improvement of the spatial resolution the peak power of the diffracted radiation remains constant if Λ is decreased, or is growing if w_0 and w_R are comparably decreased. Note, however, that reduction of w_0 is limited by the requirement mentioned above which defines efficient Bragg diffraction by a thick grating: $w_0 > \Lambda\dfrac{\lambda_P}{2\sqrt{2\lambda_R}}$. It should be also noted that with the reduction of parameters Λ and w_0 the decay time constants $\tau_a \sim \Lambda^2$ and $\tau_{tr} \sim w_0$ are also decreasing. The minimum of these time constants determines the duration of a LIG signal and, as a consequence, the number of the observed oscillation peaks of the diffraction efficiency η. Hence, the decrease of d, if needed, should be started with the reduction of that parameter, Λ or w_0, which corresponds to the larger decay time constant at given experimental conditions.

The effective length of the probe volume can be also reduced by tighter focusing of the read-out beam. In this case the result would be a sacrifice of both the LIG diffraction efficiency and the decay time constant τ_{tr}, defined now by w_R, rather than by w_0. Hence, this way of improvement of the spatial resolution looks less attractive.

4 Results and discussion

As described in Sect. 2, all the spatially resolved measurements, demonstrating the applicability of the LIGs technique to simultaneous determination of gas flow velocities and temperatures, have been performed under stationary conditions in plane submerged jets of heated air blown out of the slot nozzle into atmosphere at ambient pressure and temperature. The measurement time for a single-shot LIG signal was about 1 μs. However, the major part of signals used for the measurements have been averaged over 30 laser shots, i.e., over a time period of 1.5 s. For each flow rate there were normally three temporally-resolved signals recorded: two traces with only one of the read-out beams (R_1 or R_2) open and one informative signal proper – with both beams open. The temporal evolution of all the three signals shows a characteristic regular high-frequency oscillation structure determined by the acoustic waves excited in the probe volume. The oscillation periods are the same within 0.2%–0.3%. This oscillation decays as a result of the finite size of the pump and read-out beams, as well as because of damping of the acoustic waves. Only the signal, produced by the interfering beams S_1 and

S_2, has low-frequency modulation resulting from the Doppler shift of the signal beams frequencies. Each of two other signals, corresponding to either S_1 or S_2, is not modulated.

The examples of the temporal profile of typical single-shot and averaged LIG signals are given in Fig. 2. These signals were recorded at the jet axis near the nozzle exit ($x/h = 0.6$) and correspond to the averaged exit velocity $v_Q = 40$ m/s and $T_{ex} = 295$ K. In particular, the traces demonstrate the characteristic high- and low-frequency features of the signal profile and allow to evaluate the signal-to-noise ratio.

The Levenberg–Marquardt algorithm of non-linear fitting the temporal evolution of the signal using (6) or (7) was employed to define the parameters of interest, primarily, Ω_m and Ω. Both single-shot and averaged signals, recorded with once adjusted optical layout at various local gas flow velocities and temperatures, could be reasonably described using the same values of the parameters K and K_i. The phase shift ψ has an arbitrary value, that randomly varies with time, and thus had to be fitted for each signal independently. Observations of the averaged signal profile had shown that during a 1.5 s accumulation period the phase shift ψ was remaining practically constant. The differences of the measured data and the best fit are plotted in Fig. 2a and b (lower traces) with an offset for clarity. The deviations do not exceed 20% and 10% for single-shot and averaged signals, respectively. It is pertinent to note that for on-line single-shot measurements in turbulent-flow systems of practical interest derivation of gas flow velocities and temperatures by frequency-domain signal processing using fast Fourier transform [7–9, 19] or wavelet analysis [25] may appear to be more straightforward.

From the best fit of the averaged signal in Fig. 2b the angular frequencies $\Omega = 93.0 \pm 0.1\ \mu s^{-1}$ of the acoustic wave and $\Omega_m = 32.2 \pm 0.3\ \mu s^{-1}$ of the modulation due to the movement of the gas are deduced. With the known sound velocity in air, from Ω_m the flow velocity $v_q = 59.6 \pm 0.3$ m/s is derived. Notice that the difference between the values of v_q obtained from the single-shot and averaged signals presented as an example in Fig. 2 is of the order of 1%.

The expected proportionality between the low modulation frequency Ω_m of the LIG signal at the exit of the nozzle and the flow rate has been verified in the range of 20–200 l/min at the flow temperature $T_0 = 295$ K. The result is demonstrated in Fig. 3 by the comparison of the flow velocities v_q, derived at the jet axis at $x/h = 0.6$ from the beat frequency of the signal, with the averaged exit velocities, v_Q. Linear dependence is clearly observable, and the best-fit result $v_q = (1.48 \pm 0.03) v_Q$ is shown by the dashed line. Notice that this relation corresponds to a transversal velocity profile characteristic for a viscous plane flow inside the slot nozzle and confirms the improvement of the longitudinal spatial resolution of the present experiment, in contrast to that of [3]. There, the relation $v_q \approx 1.01 v_Q$ had been obtained for measured flow velocities, that were in fact integrated along the width of the jet. It is notable that in [19] a modification of LIG technique with a frequency-shifted reference laser beam and heterodyne signal detection [8] and a standard LDA method have been applied for comparative velocity measurements in

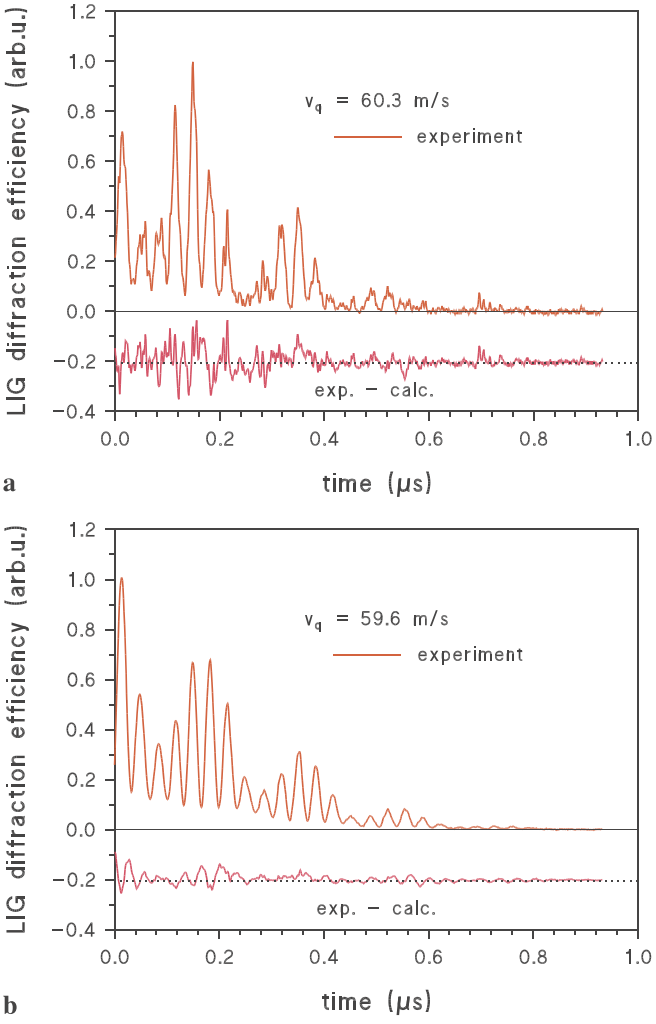

FIGURE 2 Temporal evolution of the LIG diffraction efficiency at $v_Q = 40$ m/s and ambient temperature $T_{ex} = 295$ K recorded in a single shot (**a**) and averaged over 1.5 s (**b**). The lower traces, plotted at the same vertical scale with an offset introduced for clarity, show in both cases the difference between the data and the best fit

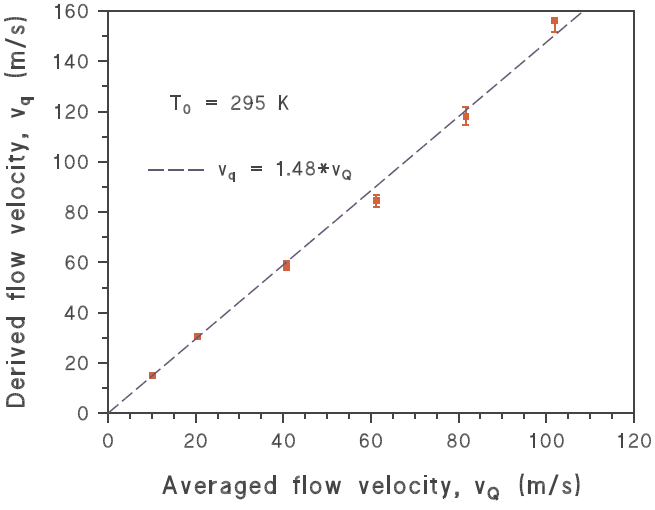

FIGURE 3 The relation between the experimentally derived flow velocities v_q near the exit of the nozzle ($x/h = 0.6$) and the averaged exit velocities v_Q, calculated from the measured flow rates and the nozzle cross-section, at the flow temperature $T_0 = 295$ K. The *dashed line* indicates the best-fit linear dependence

air jets exhausting from the similar nozzle. The results of LIG and LDA velocimetry show a reasonable agreement, and in addition are in a good correspondence with those presented in this work.

The examples of temperature measurements performed at the jet axis near the nozzle exit ($x/h = 0.6$) at different flow rates are given in Fig. 4a. The derived values are plotted against the values $T_{\rm th}$ provided by the thermocouple placed inside the flow at the position of the probe volume centre. The dashed line shows the line of equality $T = T_{\rm th}$. The observed deviations from this dependence do not exceed 3%. Flow velocities at the jet axis and $x/h = 0.6$, derived simultaneously with temperature at flow rates $Q = 24$ l/min and 80 l/min, are presented in Fig. 4b as a function of temperature given by the thermocouple. As one can expect from the mass conservation law, for a given flow rate the dependence of flow velocity on temperature should be linear: $v_q(Q, T) = v_q(Q, T_0)(T/T_0)$. This dependence is confirmed by the measurements and is illustrated in Fig. 4b by the best-fit dashed lines.

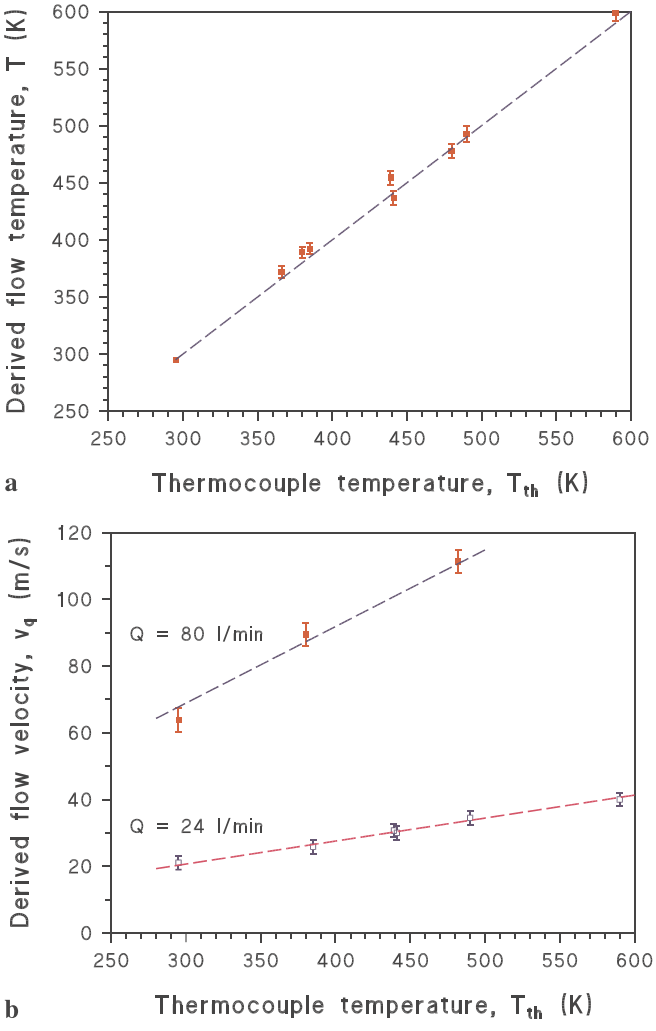

FIGURE 4 Flow parameters measured at the jet axis near the exit of the nozzle ($x/h = 0.6$) at different flow rates versus the temperature values provided by the thermocouple: (**a**) gas temperatures; the *dashed line* shows $T = T_{\rm th}$ dependence; (**b**) relative flow velocities at two flow rates; the *dashed lines* show the best-fit linear dependences of flow velocity on temperature for a given flow rate

The precision of the measured values can be estimated using standard deviations of single-shot simultaneous velocity and temperature measurements near the nozzle exit, performed under flow conditions with presumably low turbulence at the averaged exit velocity $v_Q \approx 40$ m/s. The results of these measurements presented in [5] provide $\sigma_{\rm v} = 2.5$ m/s and $\sigma_T = 1.8$ K at $T_{\rm ex} = 295$ K. It is significant that these particular numerical values are mainly defined by the noise and limited duration of LIG signals obtained, and not by turbulent velocity and temperature pulsations, that agrees with the results of comparative velocimetry using the LIGs technique and LDA [19]. In our case the signal duration was determined by the experimental conditions: the diameter of the probe volume, and gas pressure and temperature.

The achievable precision of determination of the acoustic wave period $T_{\rm a}$, and hence temperature measurements, using accumulated signals is represented by Fig. 5. Here derived values of $T_{\rm a}$ are plotted versus relative jet flow velocities $v_q/v_{\rm s0}$ measured near the nozzle exit at $T_{\rm ex} = 295$ K. The regular variation of $T_{\rm a}$ within 3% shows, however, a characteristic quadratic dependence on $v_q/v_{\rm s0}$, that obviously corresponds to the small decrease of the local sound velocity in the course of adiabatic gas expansion [20], in accordance with the relation: $T_{\rm a} = \Lambda/v_{\rm s} = T_{\rm a0}\left(\sqrt{\left(1-(\gamma-1)/2(v_q/v_{\rm s0})^2\right)}\right)^{-1}$. The dashed line in Fig. 5 shows this dependence of $T_{\rm a}$ for air ($\gamma = 1.4$).

The results of measurements of flow velocity variation along the jet axis in the range $x/h = 0.6 - 8$ at different flow rates $Q = 20$–200 l/min (and averaged exit velocities $v_Q = 10$–100 m/s, respectively) and ambient temperature $T_{\rm ex} = 295$ K are presented in Fig. 6a. The gradual decrease of v_q with the distance from the nozzle exit, the more pronounced the higher the initial velocity, can be clearly seen. The same data plotted as variations of normalized flow velocities along the jet axis (Fig. 6b) provide the possibility to observe that the increase of v_Q from 10 m/s to 20 m/s and higher results in the qualitative change of the law of velocity decrease along

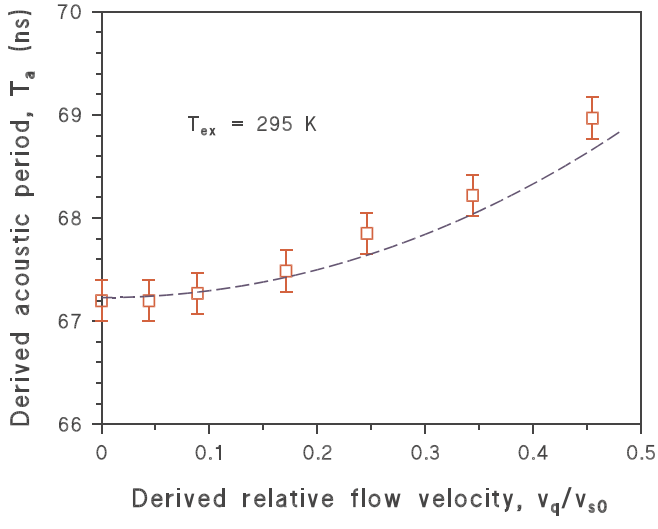

FIGURE 5 Variation of the acoustic wave period $T_{\rm a}$ with relative flow velocity $v_q/v_{\rm s0}$ measured near the nozzle exit at $T_{\rm ex} = 295$ K. The *dashed line* shows the theoretical dependence of $T_{\rm a}$

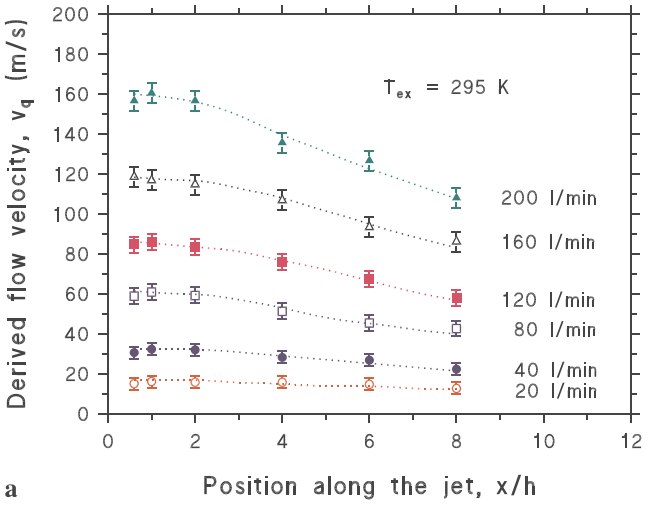

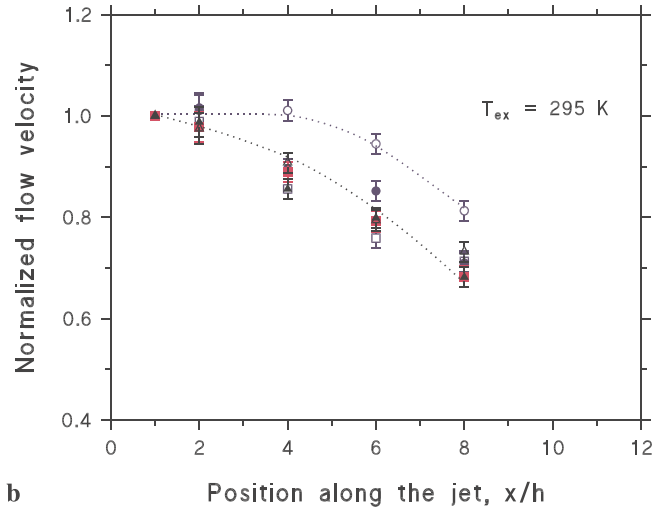

FIGURE 6 Variation of flow velocities along the jet axis at different flow rates and ambient temperature of the flow $T_{ex} = 295$ K: (**a**) absolute flow velocities; the *dotted lines* are guides for the eye; (**b**) relative flow velocities (the *symbols* are the same as in Fig. 5a); the *dotted lines* are guides for the eye

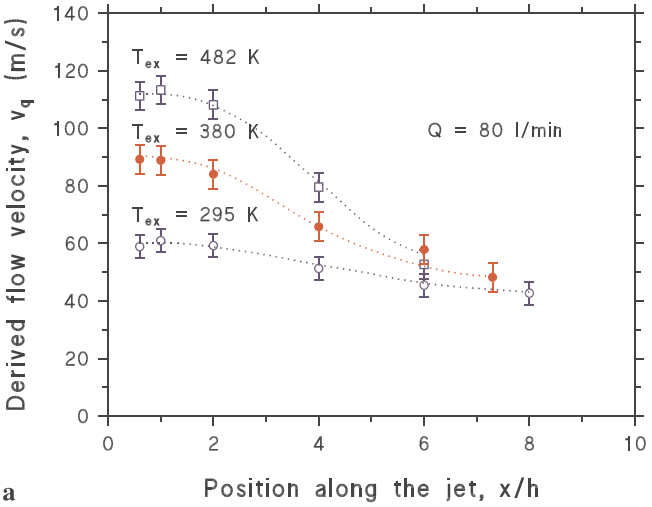

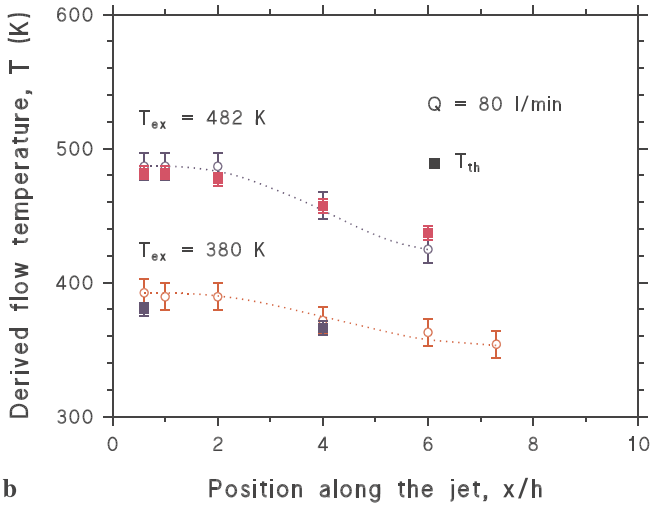

FIGURE 7 Flow parameters variation along the jet axis at different gas temperatures T_{ex} at the nozzle exit and flow rate $Q = 80$ l/min: (**a**) flow velocity; the *dotted lines* are guides for the eye; (**b**) gas temperature; the *dotted lines* are guides for the eye. Temperatures T_{th}, measured using a thermocouple inserted into a flow, are also plotted for comparison

the flow in the investigated initial part of the jet ($x/h \leq 8$). The indicated modification is probably caused by the variation of the jet characteristics from quasi-laminar to turbulent in the range of the exit velocities used, as it was anticipated in Sect. 2.

The examples of spatial distributions of flow velocities and temperatures along the jet axis, simultaneously determined in heated flows at the flow rate $Q = 80$ l/min and different temperatures T_{ex} at the nozzle exit, are presented in Fig. 7a and 7b, respectively. The faster decrease of the flow velocity with x/h along the jet axis at higher temperatures due to gas cooling is clearly observed. Temperature values T_{th}, measured using a thermocouple inserted into a flow at the centre of the LIG probe volume, are also plotted in Fig. 7b. The LIG temperature data are observed to be systematically higher than those measured by the thermocouple in the region near the nozzle exit, at $x/h \leq 2$ (see also Fig. 4a). This can be apparently ascribed, first, to the relatively large dimensions of the thermocouple tip ($\sim 1mm$) as compared to the slot height, that may result in the local cooling of the flow, and, second, to the irradiation heat losses of the thermocouple.

Distributions of flow velocity (at $T_{ex} = 295$ K) and temperature (at $T_{ex} = 380$ K) measured with a spatial resolution better than 300 µm across the jet, at positions $x/h = 1$ and $x/h = 4$, for $Q = 80$ l/min are demonstrated in Fig. 8. Both velocity profiles (see Fig. 8a) have a symmetrical shape. The characteristic modification of this shape along the flow can be observed. Notice that near the nozzle exit the distribution $v_q(z)$ is found to be parabolic, as shown by the solid line in Fig. 8a, in agreement with the transversal velocity profile of a viscous plane flow inside the channel. A small (~ 0.1 mm) but noticeable shift of the flow centre in the vertical direction, along the z-axis, with increase of x/h is an imaginary effect caused by a slight misalignment of the probe volume displacement direction and the x-axis. As observed for the transversal temperature distribution at the position $x/h = 4$ in Fig. 8b, its centre is located at the same z value as the centre of the

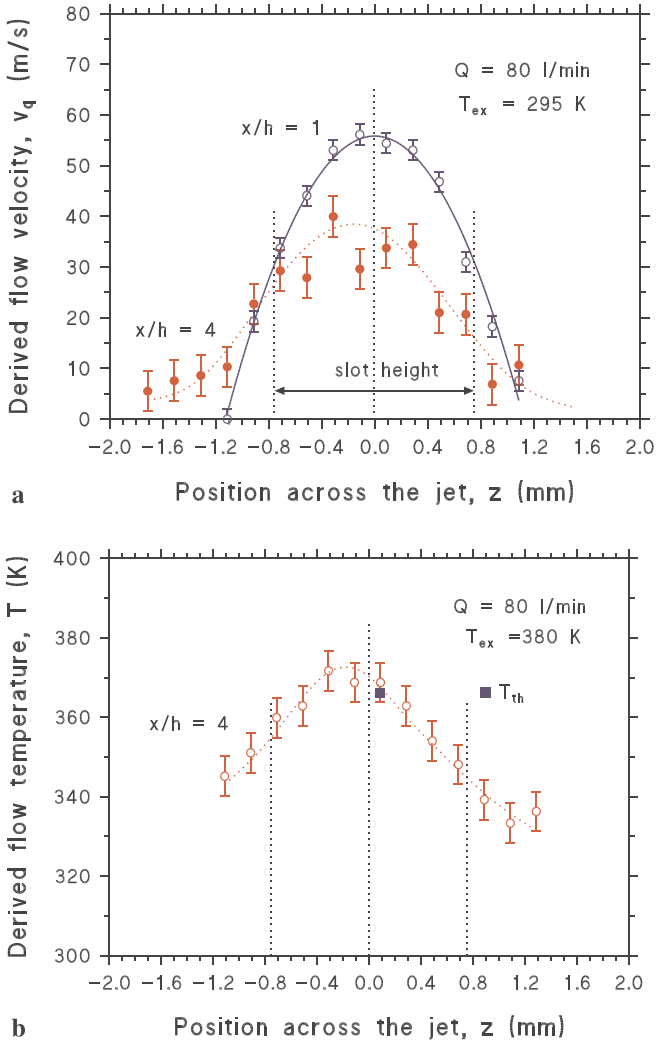

FIGURE 8 Flow parameters distributions across the jet at different x/h values for $Q = 80$ l/min: (**a**) flow velocity, $T_{ex} = 295$ K; the *solid line* shows the best-fit parabolic dependence of flow velocity v_q on z near the nozzle exit, the *dotted lines* are guides for the eye; (**b**) gas temperature, $T_{ex} = 380$ K; the *dotted line* is a guide for the eye

velocity distribution, in correspondence with the assumed jet structure of the flow.

The demonstrated longitudinal spatial resolution of the electrostrictive LIGs technique along the y-axis was estimated to be about 10 mm. This value results in spatial averaging of the derived velocity and temperature values in case of comparable flow inhomogeneity in the y-direction. To obtain higher spatial resolution, and also higher sensitivity of the velocity measurements, the angle between the read-out beam and the velocity vector should be as small as possible, that goes along with a smaller fringe spacing, Λ. Since the acoustic decay time constant τ_a of a LIG is proportional to Λ^2, it strongly decreases at a smaller Λ, that may enhance the lower limits of measurable flow velocity and temperature determination error because of a reduced amount of the observable high-frequency signal oscillation peaks.

It was observed that the decay time of the LIG signals obtained noticeably decreases, as compared to the values $\tau_a = 1.0$ µs and $\tau_{tr} \approx 0.8$–1.0 µs characteristic for the signals in quiescent air at ambient temperature and pressure, with the growth of flow velocity, as well as with even a slight increase of flow temperature above the ambient one. This reduction is observed already near the nozzle orifice, and enhances further along the jet axis. Since in our experiments $(v_q/v_{s0})^2 \ll 1$, the acoustic decay, as well as the rate of the relative displacement of the acoustic wave packets, should not noticeably depend on the flow velocity – because of the small temperature variation in the process of relatively slow movement of the gas inside the nozzle. For the same reason, the reduction of the decay time can be only partly ascribed to the appropriate variation of the parameter τ_{tr}, that accounts for the displacement of the acoustic wave packets together with the flow relative to the space-fixed probe volume.

The analysis of the recorded LIG signals shows that the faster decay of a signal can be quantitatively characterized by introducing into (2),(5) an effective exponential decay time τ, that replaces the acoustic decay constant τ_a and is used, at the fixed τ_{tr} value, as an unknown variable parameter. The values of τ derived in this way from the experimental data along the jet axis at different flow rates and ambient temperature $T_{ex} = 295$ K are presented in Fig. 9. While in the quiescent gas or at the minimal flow rate $Q = 20$ l/min the effective decay time τ is close to τ_a, it is clearly seen that it rapidly decreases with the increase of flow velocity above $v_q \approx 30$ m/s, even near the nozzle orifice ($x/h \approx 1$), i.e., at presumably the weakest turbulence conditions. The character of τ variation along the flow axis is also different for $Q = 20$ l/min and $Q \geq 40$ l/min, similar to and probably in correlation with what has been observed for the normalized flow velocities (see Fig. 6a).

The distributions of τ values across the flow at different positions x/h along the jet axis at $Q = 80$ l/min and $T_{ex} = 295$ K are presented in Fig. 10. Both transversal distributions have a quasi-symmetrical shape, correlating with the jet structure (Fig. 8a), but significantly varying along the flow axis. Near the nozzle orifice ($x/h = 1$) values of τ are higher near the flow axis, while in the regions of the boundary layers between moving and quiescent gas the distribution

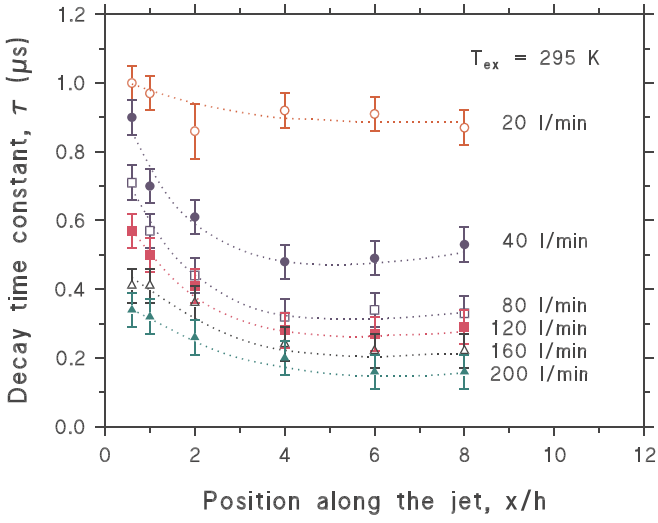

FIGURE 9 Variation of the effective decay time of the LIG signal along the jet axis at different flow rates and ambient temperature $T_{ex} = 295$ K. The *dotted lines* are guides for the eye

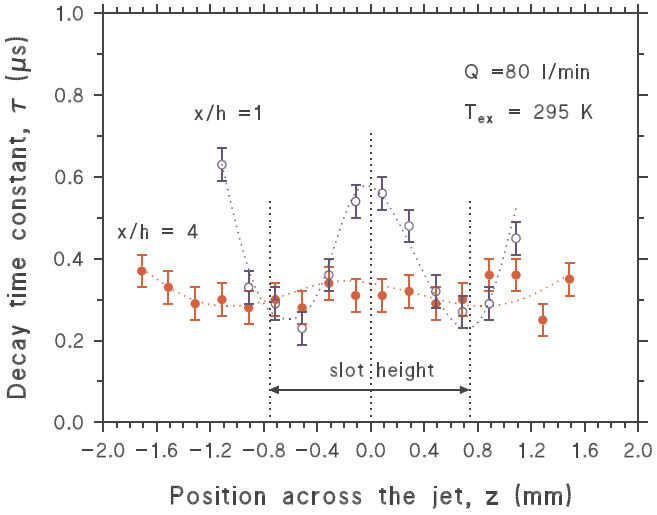

FIGURE 10 Variation of the LIG signal effective decay time across the jet at different x/h values at $Q = 80\,\mathrm{l/min}$ and ambient temperature $T_{ex} = 295\,\mathrm{K}$. The *dotted lines* are guides for the eye

has noticeable minima. Outside the jet boundaries the increase of the exponential decay time is observed. At $x/h = 4$ the distribution of τ in the central part of the flow is practically flat, with weak indications of a maximum near the flow centre and minima in the regions of the boundary layers. The values themselves are smaller than those at $x/h = 1$, despite the lower flow velocities at this distance (see Fig. 6a).

The shorter decay time of the LIG signal at elevated flow temperatures can be only partly ascribed to the decrease of τ_{tr} because of growth of sound velocity with temperature ($\tau_{tr} \sim v_s^{-1} \sim T^{-0.5}$). Additional reduction is provided by the decrease of the effective exponential decay time τ. The temperature dependence of τ at the nozzle exit ($x/h = 0.6$) is shown in Fig. 11 for two different flow rates (20 and 80 l/min). The noticeable effect of a rapid decrease of τ with temperature in the range of $T_{ex} = 295$–$500\,\mathrm{K}$ at both flow rates is stronger than could be expected from the approximate relation $\tau_a \sim T^{-1.5}$,

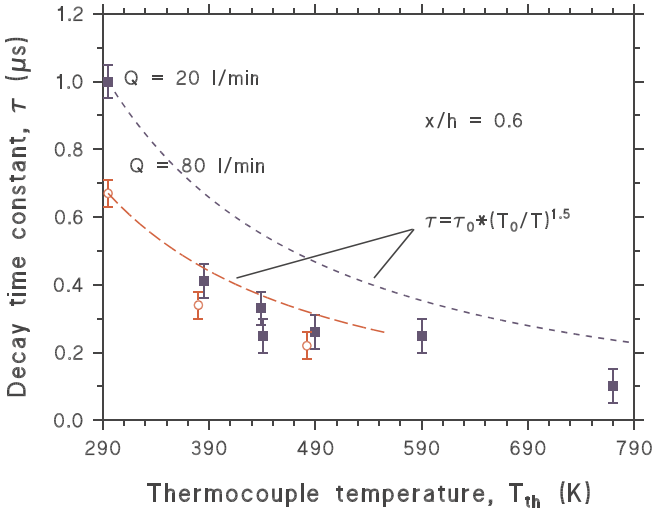

FIGURE 11 Variation of the LIG signal effective decay time at the nozzle exit with temperature T_{ex} at flow rates $Q = 20\,\mathrm{l/min}$ (*solid symbols*) and $Q = 80\,\mathrm{l/min}$ (*open symbols*). The *dashed line* shows the assumed $T^{-1.5}$ dependence of the acoustic decay time constant τ_a

with the corresponding dependences shown by dashed lines in Fig. 11. This relation accounts for the decrease of gas density inside the heated flow, as well as the weaker $T^{0.5}$ dependence of viscosity and thermal conductivity on temperature at low densities.

Obviously, the observed strong reduction of the signal decay time in a flowing gas confines the possibilities of the technique, especially in the measurements of lower flow velocities at elevated temperatures. It is reasonable to assume that it might be turbulent fluctuations in the flow, that destroy the fringes of LIGs and thus decrease the signal decay time. This conclusion is confirmed by the observed in [19] more than an order of magnitude growth of standard deviations of LDA velocity measurements with the increase of the averaged exit velocity and especially of the distance x/d from the nozzle orifice. Notice that the corresponding standard deviations of single-shot measurements using LIGs do not increase to a similar extent (see [19]), since in the v_Q and x/d ranges employed shot-to-shot variations of the derived velocities are still substantially defined by the noise and limited duration of analysed LIG signals. The question of correspondence of the experimentally derived parameters τ or standard deviations of single-shot LIG measurements with characteristics describing the turbulent movement inside the flow has to be clarified in a special investigation, either by employing a test object with known flow turbulence, or by comprising supplementary measurements (those of e.g., spectrum and mean amplitude of pressure pulsations in the flow) and numerical flow simulations.

5 Conclusion

The presented results demonstrate the applicability of the laser-induced gratings technique for non-intrusive and spatially resolved simultaneous velocity and temperature measurements in a gas flow, and provide the examples of such measurements. The realized longitudinal spatial resolution of the electrostrictive LIG technique was about 10 mm. This value gives a scale of homogeneity of flows where the technique can be efficiently applicable. A lower limit of flow velocity and upper limit of temperature, that can be measured accurately, is set by the LIG signal decay time. Consequently, the described technique might be of the most value for flows of relatively high velocity (≥ 5–$10\,\mathrm{m/s}$) and low temperatures (≤ 600–$1000\,\mathrm{K}$), with low degree of turbulence.

The results of the research also give a promise that, in addition to velocity and temperature values, spatial distribution of such a parameter as the LIG signal decay time may provide information on the turbulent movement inside the flow and on the jet structure. However, detailed analysis of the possibilities, advantages and limitations of the method demands conduction of systematic measurements using special model objects with well-characterized flow and turbulence parameters. Understanding of the availability of any additional information on flow characteristics from the LIG signals obtained would be of interest. More thorough study of the possible turbulence effects, that are assumed to limit the possibilities of the technique, is also of importance.

ACKNOWLEDGEMENTS The author is extremely grateful to Bernd Hemmerling (deceased in 2002) for fruitful cooperation during the

initial stage of this work, carried out at Paul Scherrer Institute (Villigen, Switzerland). The contribution of A.N. Klimov to the development of the software for the experimental data treatment, as well as discussions and trial experiments with O.M. Stel'makh at A.M. Prokhorov General Physics Institute (Moscow, Russia) are gratefully acknowledged. This research was supported by the Swiss Federal Department of Energy (BFE) and LEC ERCOFTAC, Switzerland.

REFERENCES

1 D.J.W. Walker, R.B. Williams, P. Ewart: Opt. Lett. **23**, 1316 (1998)
2 S. Schlamp, E.B. Cummings, H.G. Hornung: Appl. Opt. **38**, 5724 (1999)
3 D.N. Kozlov, B. Hemmerling, A. Stampanoni-Panariello: Appl. Phys. B **71**, 585 (2000)
4 S. Schlamp, E.B. Cummings, T.H. Sobota: Opt. Lett. **25**, 224 (2000)
5 B. Hemmerling, D.N. Kozlov, A. Stampanoni-Panariello: Opt. Lett. **25**, 1340 (2000)
6 S. Schlamp, E. Allen-Bradley: AIAA paper 2000-0376, January 2000
7 R.C. Hart, R.J. Balla, G.C. Herring: Appl. Opt. **40**, 965 (2001)
8 B. Hemmerling, M. Neracher, D.N. Kozlov, W. Kwan, R. Stark, D. Klimenko, W. Clauss, M. Oschwald: J. Raman Spectrosc. **33**, 912 (2002)
9 M.S. Brown, Y. Li, W.L. Roberts, J.R. Gord: Appl. Opt. **42**, 566 (2003)
10 R.B. Williams, P. Ewart, A. Dreizler: Opt. Lett. **19**, 1486 (1994)
11 M. Lefebvre, M. Péalat, J. Strempel: Opt. Lett. **17**, 1806 (1992)
12 M. Lefebvre, B. Scherrer, P. Bouchardy, T. Pot: J. Opt. Soc. Am. B **13**, 514 (1996)
13 I. Ribet, B. Scherrer, P. Bouchardy, T. Pot, J.P. Taran, M. Lefebvre: J. Raman Spectrosc. **31**, 689 (2000)
14 I. Ribet, T. Pot, M. Lefebvre: Appl. Phys. B **74**, 445 (2002)
15 A. Eder, B. Dürst, M. Jordan: Laser Doppler Velocimetry, In *Optical Measurements*, 2nd Edn. F. Mayinger, O. Feldmann (Eds.) (Springer, Berlin, Heidelberg, New York, Tokyo 2001)
16 W. Merzkirch: Particle Image Velocimetry, In *Optical Measurements*, 2nd edn, F. Mayinger, O. Feldmann (Eds.) (Springer, Berlin, Heidelberg, New York, Tokyo 2001)
17 H.J. Eichler, P. Günter, D.W. Pohl: *Laser-induced Dynamic Gratings* (Springer, Berlin, Heidelberg, New York, Tokyo, 1986)
18 A. Stampanoni-Panariello, B. Hemmerling, W. Hubschmid: Phys. Rev. A **51**, 655 (1995)
19 M. Neracher, W. Hubschmid: Appl. Phys. B **79**, 783 (2004)
20 L.D. Landau, E.M. Lifshitz: *Course of Theoretical Physics. Vol. 6. Fluid Mechanics* (Pergamon Press, Oxford, New York, Beijing, Frankfurt, Sao Paulo, Sydney, Tokio, Toronto, 1987)
21 R.B. Bird, W.E. Stewart, E.N. Lightfoot: *Transport Phenomena* (John Wiley & Sons, New York, Chichester, Brisbane, Toronto, Singapore, 2002)
22 R.B. Boyd: *Nonlinear Optics* (Academic Press, 1992)
23 W. Hubschmid, B. Hemmerling, A. Stampanoni-Panariello: J. Opt. Soc. Am. B **12**, 1850 (1995)
24 M. Born, E. Wolf: *Principles of Optics*, Chapt. 12 (Pergamon Press, Oxford, London, Edinburgh, New York, Paris, Frankfurt, 1968)
25 F. Bake, B. Lehmann: 12th International Symposium on Applications of Laser Techniques to Fluid Mechanics, 12-15 July 2004, Lisbon, Portugal